NASA TECHNICAL MEMORANDUM

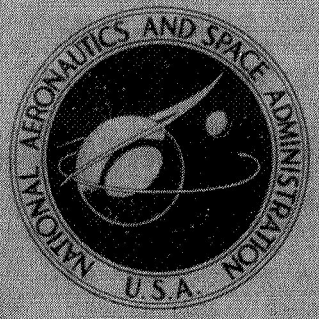

NASA TM X-2026

NASA TM X-2026

DEVICE FOR PRODUCING DYNAMIC DISTORTION PATTERNS AT INLETS OF AIR-BREATHING ENGINES

by Robert J. Baumbick

Lewis Research Center
Cleveland, Ohio 44135

NATIONAL AERONAUTICS AND SPACE ADMINISTRATION • WASHINGTON, D. C. • JUNE 1970

1. Report No. NASA TM X-2026	2. Government Accession No.	3. Recipient's Catalog No.
4. Title and Subtitle DEVICE FOR PRODUCING DYNAMIC DISTORTION PATTERNS AT INLETS OF AIR-BREATHING ENGINES		5. Report Date June 1970 6. Performing Organization Code
7. Author(s) Robert J. Baumbick		8. Performing Organization Report No. E-5402
9. Performing Organization Name and Address Lewis Research Center National Aeronautics and Space Administration Cleveland, Ohio 44135		10. Work Unit No. 720-03 11. Contract or Grant No. 13. Type of Report and Period Covered Technical Memorandum
12. Sponsoring Agency Name and Address National Aeronautics and Space Administration Washington, D. C. 20546		14. Sponsoring Agency Code

15. Supplementary Notes

16. Abstract

The development of a device for experimentally producing distortion patterns at the inlet of air-breathing engines is discussed. Both experimental and analytical results were used in defining the problems affecting system response. The analytical model was used for guidance to make modifications to the system to improve the system response.

17. Key Words (Suggested by Author(s))	18. Distribution Statement
Dynamic distortion device Inlet distortions	Unclassified - unlimited

19. Security Classif. (of this report)	20. Security Classif. (of this page)	21. No. of Pages	22. Price*
Unclassified	Unclassified	23	$3.00

*For sale by the Clearinghouse for Federal Scientific and Technical Information
Springfield, Virginia 22151

DEVICE FOR PRODUCING DYNAMIC DISTORTION PATTERNS AT INLETS OF AIR-BREATHING ENGINES

by Robert J. Baumbick

Lewis Research Center

SUMMARY

The development of the air distortion system is discussed. Also included is a discussion of the servosystem designed to drive the air valve. An analysis of the pneumatic system dynamics was made and correlated to experimental results. The objective in the design of the air distortion system was to produce pressure distortions at the engine face. This is brought about through a momentum exchange between primary air flow to the engine and secondary flow produced by the distortion valve. Problem areas that affect jet flow are cited, and corrections are suggested for improving the response. Both analytical and experimental results showed how supply line dynamics degrade the response of the system. From these results, future systems will be modified to reduce these supply line dynamics. Experimental and analytical results compared quite well for both the servosystem and the pneumatic system.

INTRODUCTION

The trend in engine development is toward increased performance without substantial increase in engine weight. Weight savings are realized by increasing the work output per stage of the compressors. The higher stage loading of these compressors results in a greater sensitivity to inlet flow distortions. Information on the effects of inlet distortion on engine performance is presented in references 1 to 3.

Because of the higher stage loading, the compressor is forced to operate closer to its stall region. Research engineers are concerned with defining the engine stall region when flow distortions are introduced to the inlet of the engine. In the past, uniform and nonuniform pressure disturbances have been produced by placing screens in the engine inlet duct. Cyclic distortions were produced with devices such as the rotating bypass valve (ref. 4) and the multispoked rotating valve (ref. 5). These devices, however, were

capable of producing only sinusoidal pressure disturbances. Since the exact nature of inlet disturbances that affect engine performance are not well defined, a more versatile tool was needed for engine distortion studies. This need led to the development of the air distortion system discussed in this report.

Six valves were installed at 60° intervals around the engine inlet duct. Figure 1(a) shows the air valves installed in the engine test chamber. Each valve discharges into nine tubes. These tubes are terminated in orifices. The discharge jets (54 total) form the array shown in figure 1(b) as it appears looking toward the engine inlet. Indicated in this figure is a sector of nine discharge jets. The system schematic, together with the location of the discharge jet plane and the pressure measuring station in the inlet duct, is shown in figure 1(c).

Pressure distortions are produced at the engine inlet through a momentum exchange between primary engine flow and secondary flow produced by the distortion system. Because each valve can be driven independently, a wide variety of pressure distortions can be produced at the engine inlet. These distortion patterns can be steady state, sinusoidal, or transient in nature. Wenzel (ref. 6) presents results of transient pressure distortions produced at the engine inlet by driving the air valves with discrete pulses. These pulses varied in both amplitude and duration. Circumferential distortion patterns from 60° to 360° in 60° sectors were produced at the engine inlet.

Meyer (ref. 7) presents results of steady-state and sinusoidal pressure distortions produced at the engine inlet. The pressure amplitudes produced at the engine inlet were attenuated beyond 20 hertz. The poor distortion patterns produced at the engine inlet at higher frequencies were the result of inlet duct dynamics and distortion system dynamics. The air distortion system performance is the subject of this report. Evaluation of the air valve and discharge jets was accomplished in bench tests using a prototype of the distortion system used in the engine test facilities.

APPARATUS AND PROCEDURE

The prototype test rig used for evaluation of the distortion system is shown in figure 2. It consists of an accumulator, supply line, air valve, and nine discharge tubes that are terminated in orifices. Pressure measurements are made at the inlet and discharge ports of the valve and at a point upstream of the discharge tube terminating orifices.

The air valve, shown in figure 3, consists of two concentric cylinders, each having 36 rectangular slots cut out on their circumference. Valve area is a linear function of the relative position between the two cylinders. A maximum valve stroke of 0.25 inch (0.635 cm) yields a flow area of 7.96 square inches (51.3 cm^2) and a flow of approxi-

mately 7 pounds per second (3.175 kg/sec). The valve is driven by a fast-response (150 to 200 Hz) two-stage electrohydraulic servovalve assembly. The servosystem was designed at the NASA Lewis Research Center and incorporates a number of unique features that extend the bandwidth of operation of the basic servovalve. More information on the design of the servosystem is presented in reference 8. The air valve position is sensed by an LVDT (linear variable differential transformer) and is used as the feedback signal for closed-loop control of the air valve.

Unbonded strain-gage pressure transducers were used for pressure measurements at the valve inlet and discharge. These were the differential pressure type and were referenced to the atmosphere. The transducers have a frequency response of better than 5 kilocycles with accuracy of better than 1 percent. A quartz-type pressure transducer was used for pressure measurements at the discharge orifice. These transducers with connecting cables have a frequency response of better than 5 kilocycles. The transducer used to measure the valve position has no dynamics in the frequency range of interest.

Steady-state data at a given operating point were taken on strip-chart recorders. Frequency responses were run by using a sweep-frequency method. A sweep rate of 1 decade per minute was used. The time-varying portions of the signals were recorded on tape. The data were reduced by the method described in reference 9, which also discusses the errors incurred in using the sweep-frequency technique.

Distortion Valve Position Servo

A block diagram of the position servo used to drive the air valve is shown in figure 4. The major components are the servoamplifier, the servovalve, and the load, which consists of the piston-in-cylinder actuator and the air valve. The first stage of the servovalve is an electrical torque motor that converts an input current into a torque. The torque actuates a flapper valve that, in turn, drives a spool valve. The spool valve directs high-pressure hydraulic fluid to the load actuator. The dynamics of the torque motor coils, due to the inductance and resistance of the coil, are included in the servoamplifier section. The second block contains the dynamic contribution from the hydromechanical portion of the servovalve. The load, consisting of the piston-in-cylinder actuator and the air valve, is represented by the expression in the third block. The mathematical expressions shown in figure 4 were developed in reference 8. The feedback transducer is represented by a constant and does not contribute any dynamics to the system over the frequency range of interest.

A transfer function relating air valve position to input signal can be obtained from figure 4 by use of standard block diagram reduction techniques. The closed-loop transfer function for the system is

$$\frac{X_v}{I} = \frac{K_1 K_2 K_4}{\left(1 + \frac{s}{\omega_1}\right)\left[s\left(\frac{s^2}{\omega_{n1}^2} + \frac{2\zeta s}{\omega_{n1}} + 1\right) + K_3\right]\left[s\left(\frac{s^2}{\omega_{n2}^2} + \frac{2\zeta s}{\omega_{n2}} + 1\right)\right] + K_1 K_2 K_4 K_{FB}} \tag{1}$$

(All symbols are defined in appendix A.) With the use of the constants for the system (listed in table I), equation (1) was evaluated over the frequency range of 1 to 200 hertz. The analytical result (fig. 5) indicates the existence of a resonance in the frequency range of interest. Later experimental tests verified the prediction of the model, and a resonance was encountered at approximately 150 hertz. This resonance was undesirable for two reasons: (1) valve damage could result because of a collision of the valve piston with its mechanical stops, and (2) for experimental testing, a constant valve stroke over the frequency range is desired. An improvement in system response was obtained through the use of a compensation network placed in the forward loop. The compensator characteristics in the frequency domain are represented by

$$G(j\omega) = \frac{1 + \frac{j\omega}{1310}}{1 + \frac{j\omega}{13\,100}} \tag{2}$$

Additional frequency response tests were run, and results showed that the compensation network did improve the system response. A comparison of valve response before and after compensation is shown in figure 6. The analytical results (dotted line) compare favorably with the actual system response.

Pneumatic System

The objective in the evaluation of the pneumatic system was to obtain large flow amplitudes from the distortion system over the frequency range of 1 to 200 hertz. A sketch of the pneumatic system appears in figure 7. The equations describing the dynamic behavior of the pneumatic system are listed in appendix B. These equations are written in terms of small perturbations about an operating point. The supply and discharge line dynamics are represented by transmission line equations developed in reference 10. The transfer function relating jet nozzle pressure or flow (terminating orifice is choked) to valve area change is developed in appendix B and is represented by

$$\frac{\frac{\tilde{P}_{tj}}{\bar{P}_{tj}}}{\frac{\tilde{A}_v}{A_v}} = \frac{\left(\frac{2\alpha_d}{1+\alpha_d}\right) e^{-\sigma_d s}\left(1 - R_i e^{-(\sigma_i+\tau_i)s}\right) K_v}{C_1 + C_2 e^{-(\sigma_i+\tau_i)s} + C_3 e^{-(\sigma_d+\tau_d)s} + C_4 e^{-(\sigma_i+\tau_i+\sigma_d+\tau_d)s}} \tag{B13}$$

The coefficients C_1, C_2, C_3, and C_4, as defined in appendix B, are

$$C_1 = 1 + K'_{p2}\alpha_i - K'_{p3}\alpha_d \tag{B14}$$

$$C_2 = -R_i(1 - K'_{p2}\alpha_i - K'_{p3}\alpha_d) \tag{B15}$$

$$C_3 = -R_d(1 + K'_{p2}\alpha_i + K'_{p3}\alpha_d) \tag{B16}$$

$$C_4 = -R_d R_i(-1 + K'_{p2}\alpha_i - K'_{p3}\alpha_d) \tag{B17}$$

and

$$R_i = \frac{1 + \alpha_i K'_{p1}}{1 - \alpha_i K'_{p1}} \tag{B9}$$

$$R_d = \frac{1 - \alpha_d}{\alpha_d + 1} \tag{B12}$$

where α, a function of Mach number in the inlet or discharge line, as developed in reference 10, is

$$\alpha = \frac{7M}{5 + M^2} \tag{B18}$$

The coefficients of the terms containing $e^{-(\sigma_i+\tau_i)s}$ represent the inlet line dynamics, and the terms containing $e^{-(\sigma_d+\tau_d)s}$ represent the discharge line dynamics in equation (B13). The constants K'_{p2} and K'_{p3} appearing in equations (B14) to (B17) represent the valve sensitivity coefficients and are developed in appendix C. The term R_i

is the inlet line reflection factor, and R_d is the discharge line reflection factor. Consider the case where $R_i = 0$, implying an impedance match for the inlet line, and the valve operating as a choked orifice (i.e., $K'_{p2} = 1$, $K'_{p3} = 0$, $K_v = 1$). Under these conditions, the coefficients of the denominator of equation (B13) become

$$C_1 = 1 + \alpha_i \tag{3}$$

$$C_2 = 0 \tag{4}$$

$$C_3 = -R_d(1 + \alpha_i) \tag{5}$$

$$C_4 = 0 \tag{6}$$

The system transfer function then reduces to

$$\frac{\dfrac{\tilde{P}_{jt}}{\bar{P}_{jt}}}{\dfrac{\tilde{A}_v}{\bar{A}_v}} = \frac{2\alpha_d e^{-\sigma_d s}}{(1 + \alpha_d)(1 + \alpha_i)\left[1 - R_d e^{-(\sigma_d + \tau_d)s}\right]} \tag{7}$$

The dynamic contributions are due to the discharge line alone and can be minimized by an impedance match in the discharge line. An impedance match is realized by allowing α_d to approach 1 (i.e., $R_d \to 0$).

An evaluation of equation (B13) over the frequency range of 1 to 200 hertz for different R_i's indicates how inlet line effects degrade system response. Figure 8 shows that large impedance mismatches in the inlet line ($R_i \to 1$) result in attenuation at frequencies of 50 and 150 hertz. The degree of attenuation is controlled by the magnitude of the impedance mismatch: In later tests run on the system, results showed that the inlet line produces severe attenuations at frequencies of 43 and 129 hertz. The discrepancy between the analytical model and the actual system can be attributed in part to the Mach number chosen for use in the model.

IMPEDANCE MATCHING

The impedance of the reflecting surface must be made equal to the transmission line

impedance in order to provide an impedance match to eliminate the reflections. An orifice that has the proper impedance when placed in the supply line will eliminate reflections. For an impedance match to exist in the supply line, R_i (eq. (B9)) must equal zero, which requires that

$$\alpha_i = -\frac{1}{K'_{p1}} \tag{8}$$

Substituting for K'_{p1} from equation (C11), with $\gamma = 1.4$, results in

$$\alpha_i = \frac{-\left[(2.4 - 2.8\,K_{p1})\left(\frac{P_{s1}}{P_{t1}}\right) - 1 + 2.8\,K_{p1}\right]}{1.4\,K_{p1}} \tag{9}$$

where K_{p1}, defined by equation (C4), is rewritten using equation (C1) and is rearranged to yield

$$C_dA = \sqrt{(0.7143 - K_{p1})\left(\frac{P_{ta}}{P_{s1}}\right)^{0.7143} \frac{\dot{W}^2 T_{ta} R}{P_{s1} P_{ta} g}} \tag{10}$$

Equation (10) yields a value of effective-orifice area that will produce an impedance match in the supply line and is seen to be a function of the operating point. Figure 9 shows the non-normalized response of jet nozzle pressure to valve area variation as a function of frequency for three different operating points. The zero-to-peak value of valve area variation was 1.6 square inches (10.3 cm^2) for all three cases. The open symbols denote the response without the impedance matching orifice. Supply line dynamics produce antiresonances at approximately 43 and 129 hertz. With the use of equations (9) and (10) and a value of $C_d = 0.6$ for the orifice, the area resulting in an impedance match for each operating point was determined. The required orifice area is included in figure 9. Later tests showed that the 4.9-square-inch- (31.6-cm^2-) area orifice produced the best dynamic results for all three cases. The solid symbols denote the improved response obtained with the orifice placed in the supply line and represent the response of the present system. The operating conditions shown in figure 9(a) result in a lower average flow but provide the largest flow variations because the valve is more effective in producing large flow variations for a given valve area change. The amplitude attenuation in the range of 10 to 60 hertz, shown by the solid symbols in figures 9(a) and (b), occurs because the orifice used is different from the computed value required for

an impedance match. The largest attenuation in the range of 10 to 60 hertz exists for the conditions of figure 9(a) because this case represents the largest mismatch. As the operating point changes (valve area increases), the degree of attenuation is reduced because the mismatch is reduced. In figure 9(c), an impedance match is achieved, and there is no attenuation in the range of 10 to 60 hertz.

Other dynamic contributions to the responses shown in figure 9 come from the discharge line, the characteristics of which are shown in figure 10. The discharge line has resonances at 55 and 165 hertz, and the amplitude of these resonances is controlled by the magnitude of R_d (eq. (B12)). The term R_d is a function of the terminating orifice used. The discharge line resonance at 165 hertz appears in the response shown in figure 9. The broad resonance at 55 hertz does not show up as well because it is close to the supply line antiresonance at 43 hertz.

CONCLUDING REMARKS

The results presented herein define the problems encountered in developing an air distortion system. The analytical models for the servo and pneumatic system provided valuable assistance in defining the problem areas and aided in determining what modifications would help to improve the response. From experience with the present system and predictions of the analytical model, certain modifications will be incorporated into a second generation system. These modifications include close coupling of the valve and accumulator and reduction of losses through reshaping the valve ports and entrances of the pneumatic system. These changes are expected to result in a flatter response of jet pressure to valve area variation over the 0- to 200-hertz frequency range of interest. In addition, the pressure levels are expected to be higher because of the reduced losses.

Lewis Research Center,
National Aeronautics and Space Administration,
Cleveland, Ohio, March 12, 1970,
720-03.

APPENDIX A

SYMBOLS

A	area, $in.^2$; m^2
a	speed of sound, ft/sec; m/sec
C_d	discharge coefficient
C_1, C_2, C_3, C_4	coefficients defined in eqs. (B14) to (B17)
$G(j\omega)$	function of frequency
g	gravitational constant, ft/sec^2; m/sec^2
I	input signal, V
K_{FB}	gain of position transducer, V/in.; V/cm
$K_{pu}, K_{pd}, K_v, K'_{pu}, K'_{pd}$	coefficients defined in eqs. (C3) and (C4) and (C9) to (C11)
K_1	variable gain of servoamplifier, A/V
K_2	constant of servovalve, in./(A)(sec); cm/(A)(sec)
K_3	constant of servovalve, sec^{-1}
K_4	gain of load driven by servovalve, sec^{-1}
L	length, in.; m
M	Mach number
P	pressure, psi; N/m^2
R	gas constant, $ft/^oR$; J/(K)(kg)
R_d	coefficient defined in eq. (B12)
R_i	coefficient defined in eq. (B9)
s	Laplace transform operator
T	absolute temperature, ^oR; K
$\dot{W}$	weight flow, lb/sec; kg/sec
X	valve position, in.; m
α	coefficient defined in eq. (B18)
γ	ratio of specific heats (1.4 for air)
ζ	damping ratio
ρ	density, lb/ft^3; kg/m^3
σ	transport time defined in eq. (B19), sec
τ	transport time defined in eq. (B20), sec
ω	frequency, sec^{-1}

Subscripts:

a, j	station locations defined in fig. 7
d	valve discharge side, downstream location
FB	position transducer
i	valve inlet side

n1	natural frequency of servovalve
n2	natural frequency of load
o	orifice
p	pressure sensitivity coefficient
s	static conditions
t	total or stagnation conditions
u	upstream location
v	valve
1, 2, 3	station locations defined in fig. 7

Superscripts:

$\bar{}$	steady state
$\sim$	perturbation
$\cdot$	time derivative
$'$	associated with constants as defined

APPENDIX B

PNEUMATIC SYSTEM DYNAMICS

Assuming constant area and accumulator pressure, flow through the orifice is given by

$$\frac{\tilde{\dot{W}}_1}{\bar{\dot{W}}_1} = K'_{p1} \frac{\tilde{P}_{t1}}{\bar{P}_{t1}} \tag{B1}$$

where K'_{p1} is defined by equation (C11).

The supply line dynamics are represented by equations developed in reference 10:

$$\frac{\tilde{P}_{t1}}{\bar{P}_{t1}} + \alpha_i \frac{\tilde{\dot{W}}_1}{\bar{\dot{W}}_1} = e^{\sigma_i s}\left(\frac{\tilde{P}_{t2}}{\bar{P}_{t2}} + \alpha_i \frac{\tilde{\dot{W}}_v}{\bar{\dot{W}}_v}\right) \tag{B2}$$

$$\frac{\tilde{P}_{t1}}{\bar{P}_{t1}} - \alpha_i \frac{\tilde{\dot{W}}_1}{\bar{\dot{W}}_1} = e^{-\tau_i s}\left(\frac{\tilde{P}_{t2}}{\bar{P}_{t2}} - \alpha_i \frac{\tilde{\dot{W}}_v}{\bar{\dot{W}}_v}\right) \tag{B3}$$

The linearized equation representing the valve is

$$\frac{\tilde{\dot{W}}_v}{\bar{\dot{W}}_v} = K_v \frac{\tilde{A}_v}{\bar{A}_v} + K'_{p2} \frac{\tilde{P}_{t2}}{\bar{P}_{t2}} + K'_{p3} \frac{\tilde{P}_{t3}}{\bar{P}_{t3}} \tag{B4}$$

where K_v, K'_{p2}, and K'_{p3} are defined by equations (C9) to (C11). Discharge line dynamics are

$$\frac{\tilde{P}_{tj}}{\bar{P}_{tj}} + \alpha_d \frac{\tilde{\dot{W}}_j}{\bar{\dot{W}}_j} = e^{-\sigma_d s}\left(\frac{\tilde{P}_{t3}}{\bar{P}_{t3}} + \alpha_d \frac{\tilde{\dot{W}}_v}{\bar{\dot{W}}_v}\right) \tag{B5}$$

$$\frac{\tilde{P}_{tj}}{\bar{P}_{tj}} - \alpha_d \frac{\tilde{\dot{W}}_j}{\bar{\dot{W}}_j} = e^{\tau_d s}\left(\frac{\tilde{P}_{t3}}{\bar{P}_{t3}} - \alpha_d \frac{\tilde{\dot{W}}_v}{\bar{\dot{W}}_v}\right) \tag{B6}$$

The terminating orifice that operates as a choked station is represented by

$$\frac{\tilde{\dot{W}}_j}{\bar{\dot{W}}_j} = \frac{\tilde{P}_{tj}}{\bar{P}_{tj}} \tag{B7}$$

Substituting equation (B1) into (B2) and substituting the result into (B3) yields

$$\frac{\tilde{P}_{t2}}{\bar{P}_{t2}} = -\alpha_i \left[\frac{1 + R_i e^{-(\sigma_i+\tau_i)s}}{1 - R_i e^{-(\sigma_i+\tau_i)s}} \right] \frac{\tilde{\dot{W}}_v}{\bar{\dot{W}}_v} \tag{B8}$$

where

$$R_i = \frac{1 + \alpha_i K'_{p1}}{1 - \alpha_i K'_{p1}} \tag{B9}$$

Substituting equation (B8) into (B4) and rearranging results in

$$\frac{\tilde{\dot{W}}_v}{\bar{\dot{W}}_v} \left[\frac{1 + K'_{p2}\alpha_i - R_i(1 - K'_{p2}\alpha_i)e^{-(\sigma_i+\tau_i)s}}{1 - R_i e^{-(\sigma_i+\tau_i)s}} \right] = K_v \frac{\tilde{A}_v}{\bar{A}_v} + K'_{p3} \frac{\tilde{P}_{t3}}{\bar{P}_{t3}} \tag{B10}$$

Substituting equation (B7) into (B6) to eliminate $\tilde{\dot{W}}_j/\bar{\dot{W}}_j$ and then substituting this result and (B7) into (B5) to eliminate $\tilde{P}_{t3}/\bar{P}_{t3}$ and $\tilde{\dot{W}}_j/\bar{\dot{W}}_j$ yields

$$\frac{\tilde{\dot{W}}_v}{\bar{\dot{W}}_v} = \left(\frac{1 + \alpha_d}{2\alpha_d} \right) e^{\sigma_d s} \left[1 - R_d e^{-(\sigma_d+\tau_d)s} \right] \frac{\tilde{P}_{tj}}{\bar{P}_{tj}} \tag{B11}$$

where

$$R_d = \frac{1 - \alpha_d}{1 - \alpha_d} \tag{B12}$$

Simultaneous solution of equations (B5), (B6), (B10), and (B11) to eliminate $\tilde{P}_{t3}/\bar{P}_{t3}$

and $\tilde{\dot{W}}_v/\bar{\dot{W}}_v$ results in the final equation which represents the response of jet nozzle pressure to valve area variation.

$$\frac{\frac{\tilde{P}_{tj}}{\bar{P}_{tj}}}{\frac{\tilde{A}_v}{\bar{A}_v}} = \frac{\left(\frac{2\alpha_d}{1+\alpha_d}\right)e^{-\sigma_d s}K_v\left[1 - R_i e^{-(\sigma_i+\tau_i)s}\right]}{C_1 + C_2 e^{-(\sigma_i+\tau_i)s} + C_3 e^{-(\sigma_d+\tau_d)s} + C_4 e^{-(\sigma_i+\tau_i+\sigma_d+\tau_d)s}} \tag{B13}$$

where

$$C_1 = 1 + \alpha_i K'_{p2} - \alpha_d K'_{p3} \tag{B14}$$

$$C_2 = -R_i(1 - K'_{p2}\alpha_i - K'_{p3}\alpha_d) \tag{B15}$$

$$C_3 = -R_d(1 + K'_{p2}\alpha_i + K'_{p3}\alpha_d) \tag{B16}$$

$$C_4 = -R_d R_i(-1 + K'_{p2}\alpha_i - K'_{p3}\alpha_d) \tag{B17}$$

and α, σ, and τ, as defined in reference 10, are

$$\alpha = \frac{1.4M}{1 + 0.2M^2} \tag{B18}$$

$$\sigma = \frac{\frac{L}{a}}{1 + M} \tag{B19}$$

$$\tau = \frac{\frac{L}{a}}{1 - M} \tag{B20}$$

APPENDIX C

VALVE SENSITIVITY COEFFICIENTS

Compressible flow through an unchoked orifice is represented by

$$\dot{W} = \sqrt{\frac{2g\gamma}{R(\gamma - 1)}}\, C_d \frac{A_o P_{tu}}{\sqrt{T_{tu}}} \left(\frac{P_{sd}}{P_{tu}}\right)^{1/\gamma} \sqrt{1 - \left(\frac{P_{sd}}{P_{tu}}\right)^{(\gamma-1)/\gamma}} \tag{C1}$$

The following expression is obtained by linearization of equation (C1):

$$\frac{\tilde{\dot{W}}}{\bar{\dot{W}}} = \frac{\tilde{A}_o}{\bar{A}_o} + K_{pu} \frac{\tilde{P}_{tu}}{\bar{P}_{tu}} + K_{pd} \frac{\tilde{P}_{sd}}{\bar{P}_{sd}} \tag{C2}$$

where

$$K_{pu} = \left(\frac{\gamma - 1}{\gamma}\right) \left\{ 1 + \frac{\left(\frac{P_{sd}}{P_{tu}}\right)^{(\gamma-1)/\gamma}}{2\left[1 - \left(\frac{P_{sd}}{P_{tu}}\right)^{(\gamma-1)/\gamma}\right]} \right\} \tag{C3}$$

$$K_{pd} = \frac{1}{\gamma} \left\{ 1 - \frac{(\gamma - 1)}{2} \frac{\left(\frac{P_{sd}}{P_{tu}}\right)^{(\gamma-1)/\gamma}}{\left[1 - \left(\frac{P_{sd}}{P_{tu}}\right)^{(\gamma-1)/\gamma}\right]} \right\} \tag{C4}$$

For consistency, equation (C2) should contain a total downstream pressure. The expression for total pressure at a point is given by

$$P_{td} = P_{sd} + \frac{\dot{W}^2}{2g\rho_{sd}A_d^2} \tag{C5}$$

The orifice loss assumed for this valve is taken care of by assuming that static pressure is constant over the mixing region downstream of the valve. Equation (C5) is valid for low Mach numbers in the pipe downstream of the valve.

From the continuity equation, orifice flow is equal to downstream flow. From perfect gas law,

$$\frac{P_{sd}}{\rho_{sd}^{\gamma}} = \text{constant} \tag{C6}$$

Substituting equation (C6) into (C5) to eliminate ρ_{sd} and then linearizing the result yields

$$\frac{\tilde{P}_{sd}}{\bar{P}_{sd}} = \left[\frac{\gamma \bar{P}_{td}}{(\gamma+1)\bar{P}_{sd} - \bar{P}_{td}}\right]\frac{\tilde{P}_{td}}{\bar{P}_{td}} - \left[\frac{2\gamma(\bar{P}_{td} - \bar{P}_{sd})}{(\gamma+1)\bar{P}_{sd} - \bar{P}_{td}}\right]\frac{\tilde{\dot{W}}}{\bar{\dot{W}}} \tag{C7}$$

Substituting equation (C7) into (C2) and rearranging terms results in

$$\frac{\tilde{\dot{W}}}{\bar{\dot{W}}} = K_v \frac{\tilde{A}_o}{\bar{A}_o} + K'_{pu}\frac{\tilde{P}_{tu}}{\bar{P}_{tu}} + K'_{pd}\frac{\tilde{P}_{td}}{\bar{P}_{td}} \tag{C8}$$

where

$$K_v = \frac{\left[(\gamma+1)\left(\frac{P_{sd}}{P_{td}}\right) - 1\right]}{\left\{\left[(\gamma+1) - 2\gamma K_{pd}\right]\frac{P_{sd}}{P_{td}} - (1 - 2\gamma K_{pd})\right\}} \tag{C9}$$

$$K'_{pu} = K_{pu}\left(\frac{\left[(\gamma+1)\left(\frac{P_{sd}}{P_{td}}\right) - 1\right]}{\left\{\left[(\gamma+1) - 2\gamma K_{pd}\right]\frac{P_{sd}}{P_{td}} - (1 - 2\gamma K_{pd})\right\}}\right) \tag{C10}$$

$$K'_{pd} = \frac{\gamma K_{pd}}{\left\{\left[(\gamma + 1) - 2\gamma K_{pd}\right] \frac{P_{sd}}{P_{td}} - (1 - 2\gamma K_{pd})\right\}} \tag{C11}$$

where K_{pu} and K_{pd} are defined in equations (C3) and (C4). For a choked orifice, equation (C1) is

$$\dot{W} = \sqrt{\frac{g\gamma}{R\left(\frac{\gamma + 1}{2}\right)^{(\gamma+1)/(\gamma-1)}}} \frac{C_d A_o P_{tu}}{\sqrt{T_{tu}}} \tag{C12}$$

and (C2) to (C4) become

$$\frac{\tilde{\dot{W}}}{\bar{\dot{W}}} = \frac{\tilde{A}_o}{\bar{A}} + \frac{\tilde{P}_{tu}}{\bar{P}_{tu}} \tag{C13}$$

$$K_{pu} = 1 \tag{C14}$$

$$K_{pd} = 0 \tag{C15}$$

and (C9) to (C11) become

$$K_v = 1 \tag{C16}$$

$$K'_{pu} = 1 \tag{C17}$$

$$K'_{pd} = 0 \tag{C18}$$

REFERENCES

1. Alford, J. S.: Inlet Duct - Engine Flow Compatability. Proceedings of the 5th International Aeronautical Conference. Inst. Aeron. Sci., 1955, pp. 504-519.

2. Alford, Joseph S.: Inlet Flow Distortion Index. Journées Internationalees de Sciences Aéronautiques, Paris, May 27-29, 1957, pp. 71-94.

3. Conrad, E. William; Hanson, Morgan P.; and McAulay, John E.: Effect of Inlet-Air-Flow Distortion on Steady-State Altitude Performance of an Axial-Flow Turbojet Engine. NACA RM E55A04, 1955.

4. Wasserbauer, Joseph F.; and Whipple, Daniel L.: Experimental Investigation of the Dynamic Response of a Supersonic Inlet to External and Internal Disturbances. NASA TM X-1648, 1968.

5. Gabriel, D.; Wallner, L.; Lubick, R.; and Vasu, G.: Some Effects of Inlet Pressure and Temperature Transients on Turbojet Engines. Aeron. Eng. Rev., vol. 16, no. 9, Sept. 1957, pp. 54-59, 68.

6. Wenzel, Leon M.: Experimental Investigation of the Effects of Pulse Pressure Distortions Imposed on the Inlet of a Turbofan Engine. NASA TM X-1928, 1969.

7. Meyer, Carl L.; McAulay, John E.; and Biesiadny, Thomas J.: Technique for Inducing Controlled Steady-State and Dynamic Inlet Pressure Disturbances for Jet Engine Tests. NASA TM X-1946, 1970.

8. Zeller, John R.: Analysis of Dynamic Performance Limitations of Fast Response (150 to 200 Hz) Electrohydraulic Servos. NASA TN D-5388, 1969.

9. Drain, Daniel I.; Burton, William M.; and Paulovich, Francis J.: Airbreathing Propulsion System Testing Using Sweep Frequency Techniques. NASA TN D-5485, 1969.

10. Willoh, Ross G.: A Mathematical Analysis of Supersonic Inlet Dynamics. NASA TN D-4969, 1968.

TABLE I. - CONSTANTS FOR SERVOSYSTEM

Variable gain of servoamplifier, K_1, A/V	
Servovalve constant, K_2, in./(A)(sec); cm/(A)(sec)	623; 1580
Servovalve constant, K_3, sec^{-1}	840
Constant associated with load, K_4, sec^{-1}	7290; 7290
Position transducer, K_{FB}, V/in.; V/cm	80; 31.5
Corner frequency of servoamplifier, ω_1, sec^{-1}	17 000
Natural frequency of servovalve, ω_{n1}, sec^{-1}	4600
Natural frequency of load, ω_{n2}, sec^{-1}	5040
Damping ratio of servovalve, ζ_1	0.4
Damping ratio of load, ζ_2	0.186

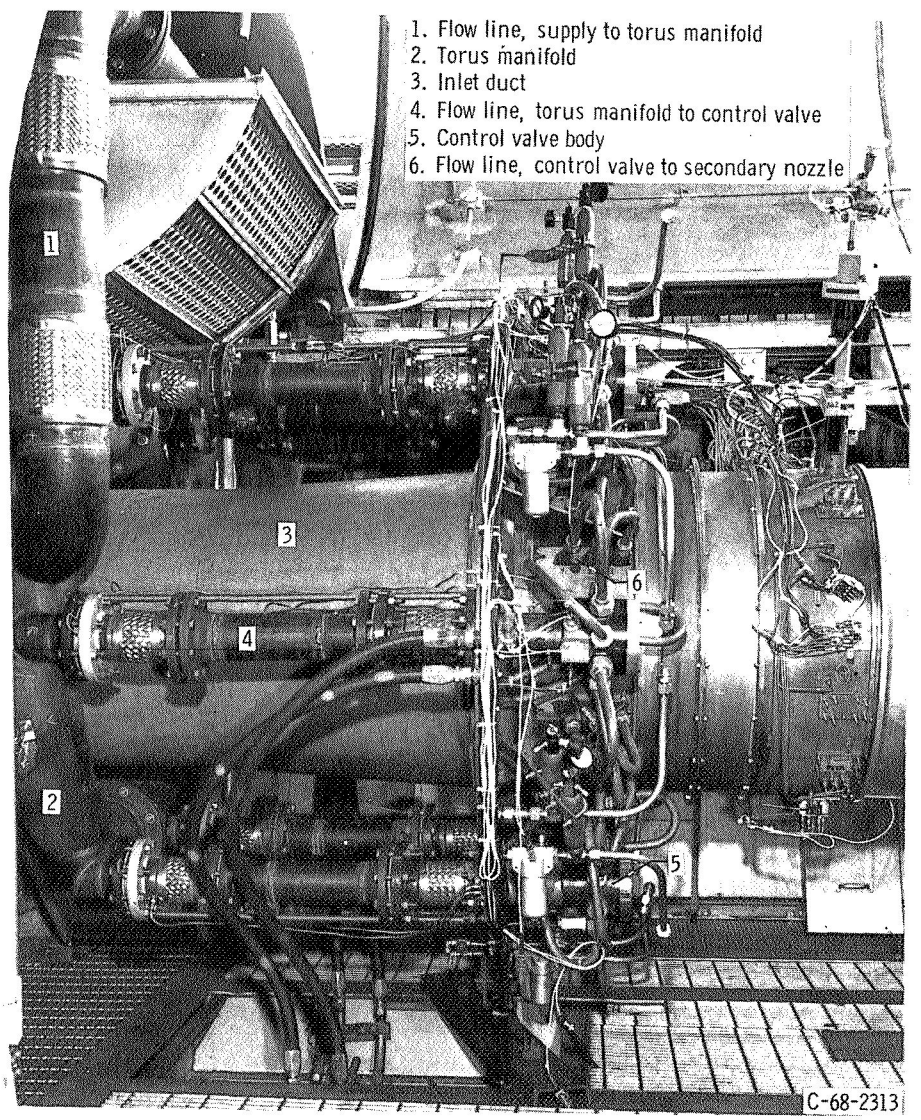

(a) Installation of air distortion valves in test chamber.

Figure 1. - Facility installation.

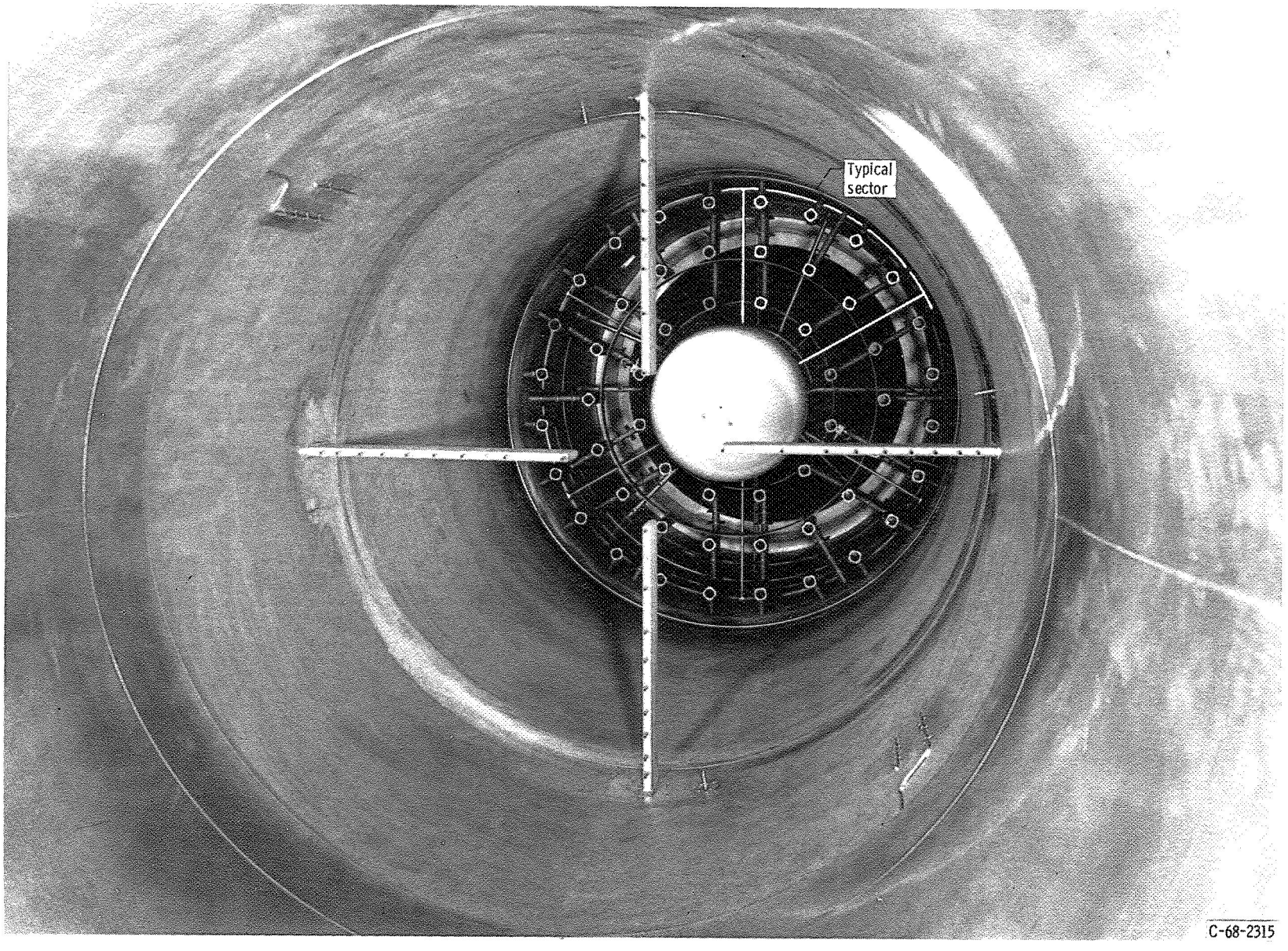

(b) Array of distortion jets in inlet duct.

Figure 1. - Continued.

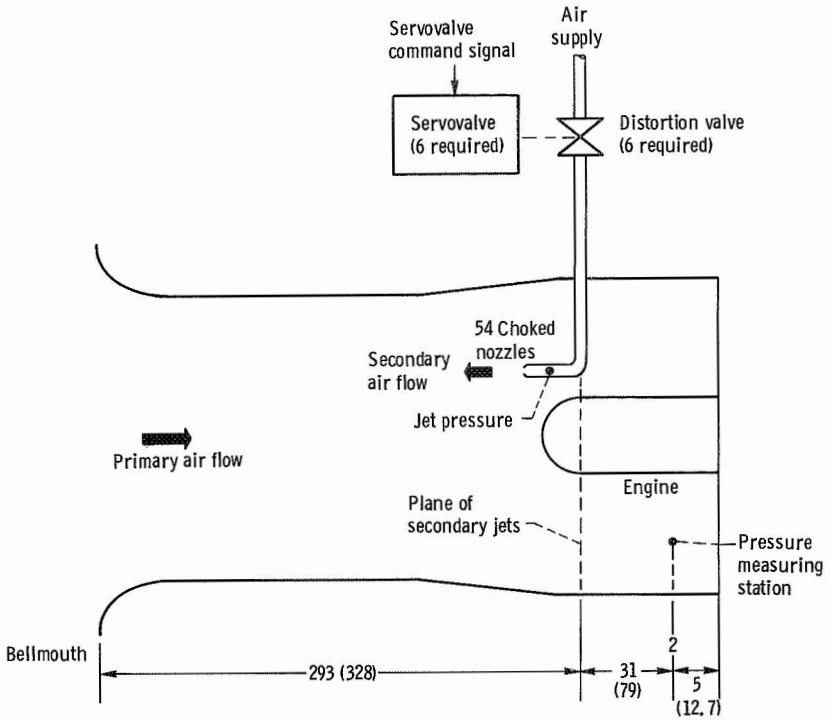

(c) Location of jets in engine inlet duct (all dimensions are in inches (cm)).

Figure 1. - Concluded.

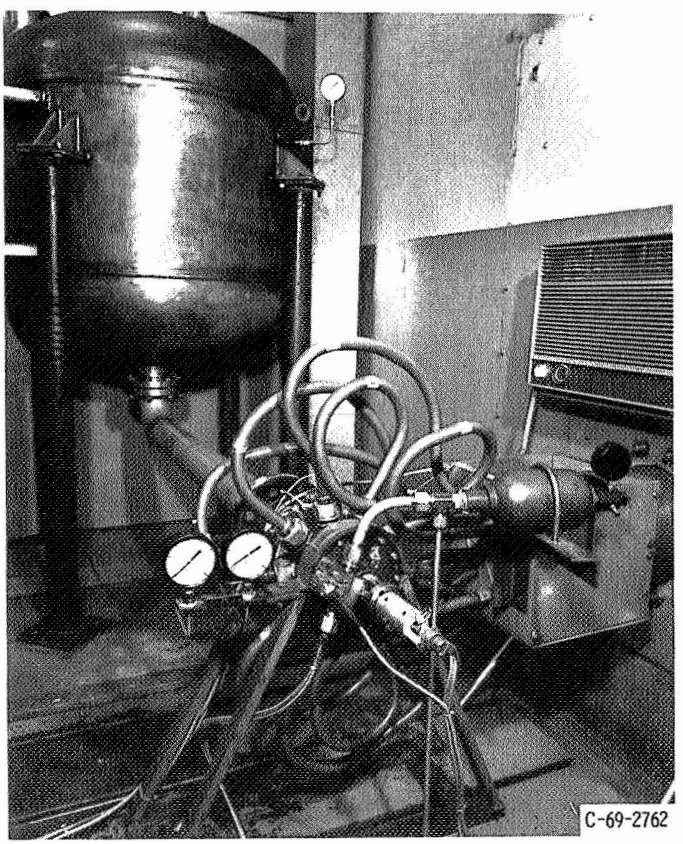

Figure 2. - Prototype air valve setup.

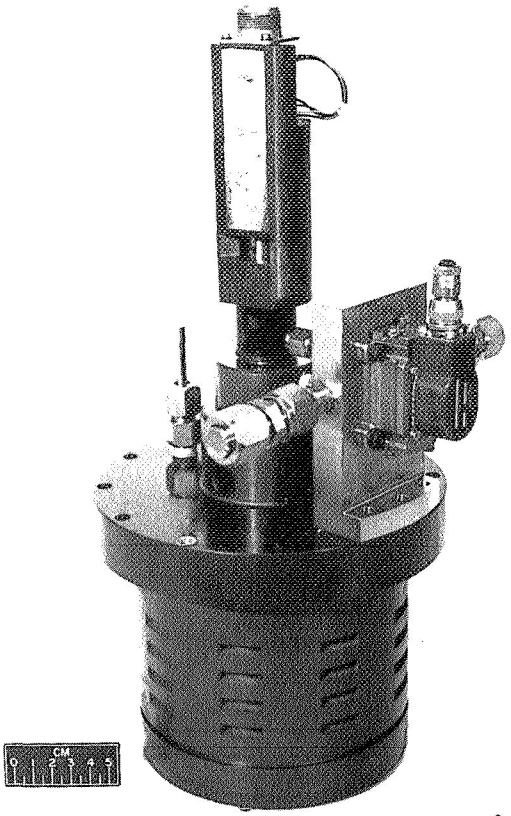

C-68-2312

Figure 3. - Air valve piston-cylinder assembly.

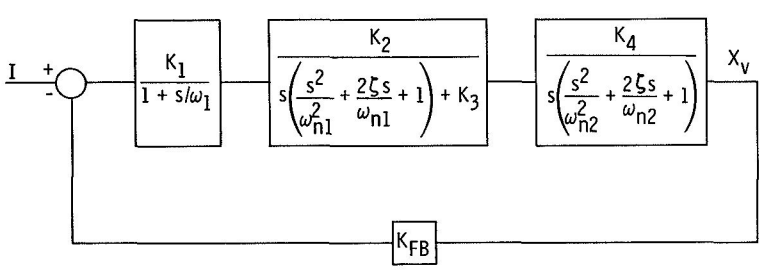

Figure 4. - Dynamics of air valve position servo.

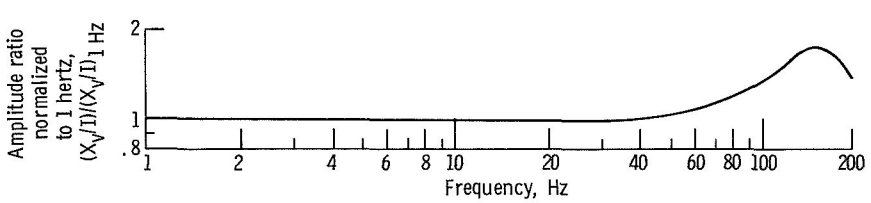

Figure 5. - Effect of gain on air valve response (analytical model).

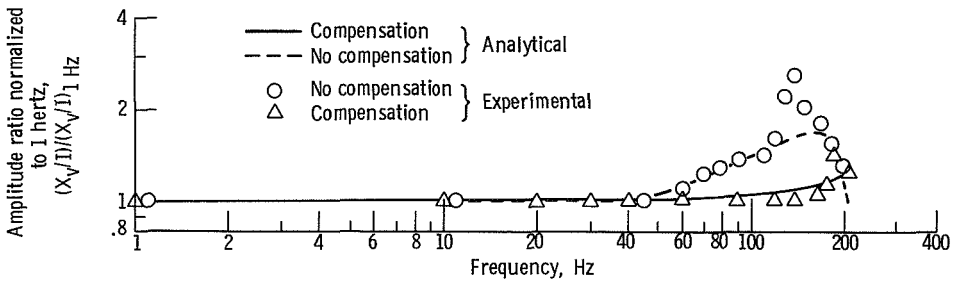

Figure 6. - Effect of compensation on air valve response.

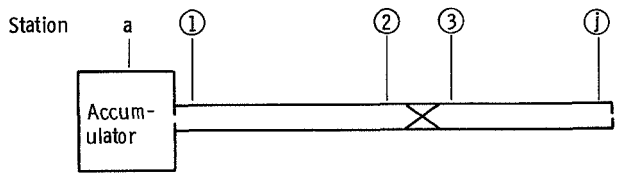

Figure 7. - Pneumatic system for air valve. Inlet line: length, 66 inches (168 cm); outside diameter, 4 inches (10.16 cm); discharge line (total of nine): length, 40 inches (101.6 cm); outside diameter, 1 inch (2.54 cm).

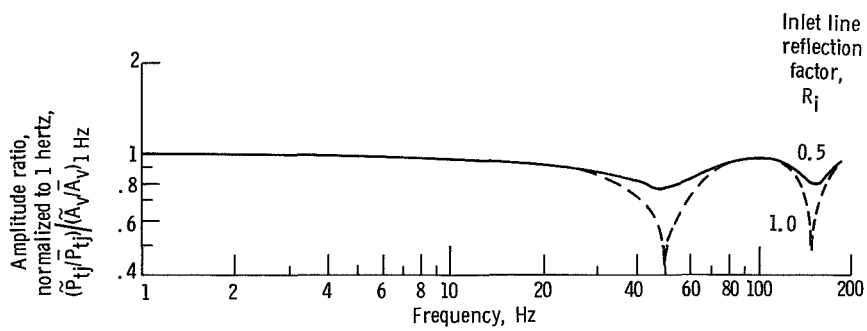

Figure 8. - Effect of inlet line dynamics on system response for analytical model.

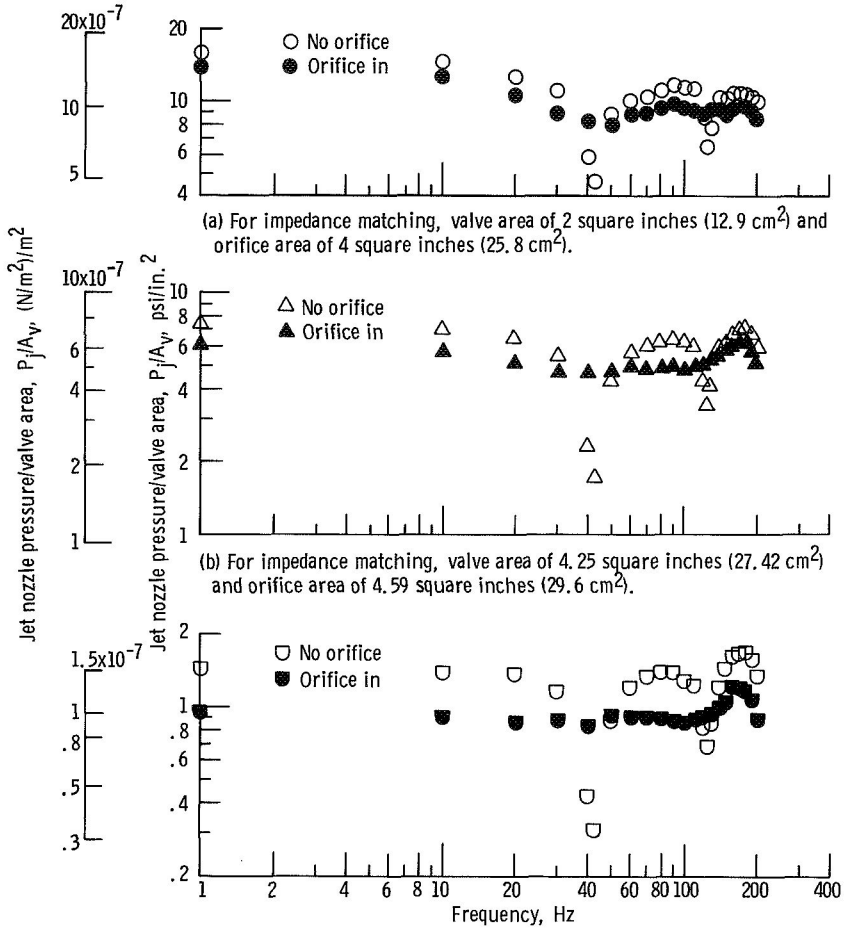

(a) For impedance matching, valve area of 2 square inches (12.9 cm^2) and orifice area of 4 square inches (25.8 cm^2).

(b) For impedance matching, valve area of 4.25 square inches (27.42 cm^2) and orifice area of 4.59 square inches (29.6 cm^2).

(c) For impedance matching, valve area of 6.3 square inches (40.65 cm^2) and orifice area of 4.9 square inches (31.6 cm^2).

Figure 9. - Experimental results illustrating improved response obtained with impedance matching orifice in supply line.

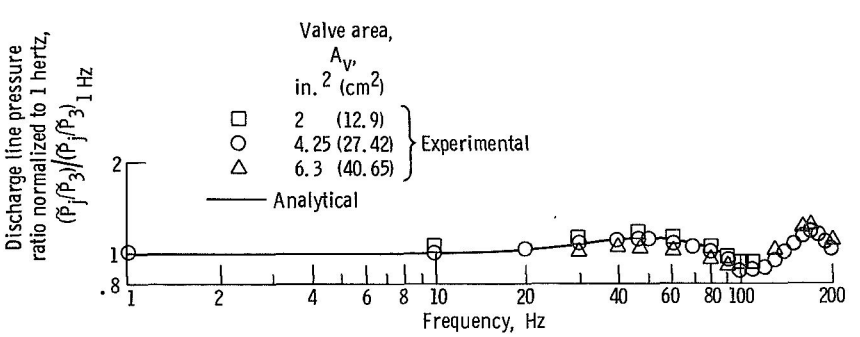

Figure 10. - Comparison of analytical and experimental results for discharge tubes.

"The aeronautical and space activities of the United States shall be conducted so as to contribute . . . to the expansion of human knowledge of phenomena in the atmosphere and space. The Administration shall provide for the widest practicable and appropriate dissemination of information concerning its activities and the results thereof."

—NATIONAL AERONAUTICS AND SPACE ACT OF 1958

NASA SCIENTIFIC AND TECHNICAL PUBLICATIONS

TECHNICAL REPORTS: Scientific and technical information considered important, complete, and a lasting contribution to existing knowledge.

TECHNICAL NOTES: Information less broad in scope but nevertheless of importance as a contribution to existing knowledge.

TECHNICAL MEMORANDUMS: Information receiving limited distribution because of preliminary data, security classification, or other reasons.

CONTRACTOR REPORTS: Scientific and technical information generated under a NASA contract or grant and considered an important contribution to existing knowledge.

TECHNICAL TRANSLATIONS: Information published in a foreign language considered to merit NASA distribution in English.

SPECIAL PUBLICATIONS: Information derived from or of value to NASA activities. Publications include conference proceedings, monographs, data compilations, handbooks, sourcebooks, and special bibliographies.

TECHNOLOGY UTILIZATION PUBLICATIONS: Information on technology used by NASA that may be of particular interest in commercial and other non-aerospace applications. Publications include Tech Briefs, Technology Utilization Reports and Notes, and Technology Surveys.

Details on the availability of these publications may be obtained from:

SCIENTIFIC AND TECHNICAL INFORMATION DIVISION

NATIONAL AERONAUTICS AND SPACE ADMINISTRATION

Washington, D.C. 20546